Scanning tunnelling microscopy study of the charge-density wave in Hf-doped 1T-TaS_2

2000 J. Phys.: Condens. Matter 12 4353

(http://iopscience.iop.org/0953-8984/12/19/306)

J. Phys.: Condens. Matter **12** (2000) 4353–4363. Printed in the UK PII: S0953-8984(00)09154-2

Scanning tunnelling microscopy study of the charge-density wave in Hf-doped 1T-TaS_2

H Bando†, K Koizumi†, Y Miyahara‡ and H Ozaki†

† Department of Electrical, Electronic and Computer Engineering, Waseda University, Ohkubo 3-4-1, Shinjuku-ku, Tokyo, 169-8555, Japan

‡ Department of Microengineering, Swiss Federal Institute of Technology Lausanne (EPFL), CH-1015 Lausanne, Switzerland

Received 1 November 1999, in final form 21 February 2000

Abstract. The effect of doping with Hf atoms on the nearly commensurate (NC) charge-density-wave (CDW) structures of 1T-TaS_2 was investigated using scanning tunnelling microscopy (STM) at room temperature, for levels of substitution of Hf for Ta up to 6.9%. It was found that the Hf atom introduces a point defect to the CDW superlattice at the CDW domain boundary for lower contents. For Hf contents higher than 1%, the CDW superlattice melted and a distorted structure was observed instead of the usual CDW superlattice. The change of the CDW structure observed by STM was compared with the change of the ρ–T characteristics.

1. Introduction

Since the charge-density-wave (CDW) state was discovered by Wilson *et al* in the transition metal dichalcogenides [1], many studies of CDWs have been made on these materials. Among the many transition metal dichalcogenides, 1T-TaS_2 is one of the most studied materials owing to its unique characteristics, such as it having a nearly commensurate (NC) CDW phase and a triclinic (T) CDW phase in the temperature range between the incommensurate (I) and the commensurate (C) CDW phases [2, 3]. The T phase exists only upon warming. The CDW amplitude in 1T-TaS_2 is so strong that the CDW energy gap is opened along the whole Fermi surface in the commensurate phase, showing a semiconductor-like behaviour in the resistivity–temperature characteristics at low temperature [1, 4–6]. The studies on the CDW structure of the NC phase have progressed by usage of scanning tunnelling microscopy (STM) and it has been established that the NC phase has a hexagonal domain structure of the CDW in which the CDW is commensurate with the atomic lattice, and has one-lattice-period phase shifts between the CDWs in adjacent domains [7, 8].

The occurrence of the CDW is related to the nesting condition of the Fermi surface, and thus its shape in the absence of a CDW (normal state). The Fermi surface of the transition metal dichalcogenides in the normal state is made up of the d electrons of the transition metal. In 1T-TaS_2, the Fermi surface is made up of the Ta 5d electrons and its shape is tubular [1], which is advantageous to the nesting. Substitution of a suitable element for Ta in 1T-TaS_2 causes a change in the size of the Fermi surface, and thus, through a change in the nesting condition, produces a change in the CDW structure. Many works on substitutions for the cation or the anion have been carried out for various systems by using the transport properties [4, 9, 10], electron diffraction [1] and STM [11–13]. The number of 3d electrons in a Ti atom is less

0953-8984/00/194353+11$30.00

by one than that of 5d electrons in a Ta atom when substituted in 1T-TaS_2. The energy levels of 3d orbitals in a Ti atom are close to those of 5d orbitals in a Ta atom [14], and the Ti–S bond length (0.242 nm in 1T-TiS_2 [15]) is also close to the Ta–S bond length (0.244 nm in 1T-TaS_2 [15]). Thus, a strong hybridization of these two orbitals is expected. Studies of Ti substitution for Ta in 1T-TaS_2 were carried out and its effects were explained by the effect of the shrinkage of the Fermi surface on the nesting condition [1].

Although Hf belongs to the same column of the periodic table as Ti, the Hf–S bond length (0.256 nm in 1T-HfS_2 [15]) is different to the Ta–S bond length in 1T-TaS_2, and the energy levels of the 5d orbitals of a Hf atom are higher than those for a Ta atom [14], in contrast to the case for Ti. There have been very few investigations of Hf substitution in 1T-TaS_2 [4, 16, 17].

In the present study, we investigate the effect of Hf substitution for Ta in 1T-TaS_2, aiming to observe a local effect on the NC-CDW structure, in contrast to the case for Ti substitution, by means of STM.

2. Experimental methods

Powders of Ta, Hf and S with a specified stoichiometric ratio were sealed into a quartz ampoule at about 8×10^{-4} Pa. The ampoule was heated in an electric furnace for 92 hours at 920 °C and $Ta_{1-x}Hf_xS_2$ polycrystalline powder was obtained. The polycrystalline powder was sealed into a quartz ampoule again with powder with excess S ($\sim$1 mg cm^{-3}) and the agent I_2 ($\sim$5 mg cm^{-3}) at about 8×10^{-4} Pa. The ampoule was heated in the furnace for more than 130 hours with a temperature gradient of about 10 °C cm^{-1} and the growth zone temperature of 900 °C for the single-crystal growth. We checked that the Hf atoms were not segregated in the single crystals by means of an electron probe microanalyser (EPMA). The atomic ratio in the single crystals was determined by inductively coupled plasma spectrometry (ICP). The Hf concentrations x of $Ta_{1-x}Hf_xS_2$ used in this study were 0, 0.0003, 0.0016, 0.010, 0.035, 0.046 and 0.069. The temperature dependence of the resistivity for the $Ta_{1-x}Hf_xS_2$ single crystals was measured by means of the conventional van der Pauw method in the temperature region 10–365 K. The speed of the temperature increase and decrease was within 1 K min^{-1}.

The CDW structure in $Ta_{1-x}Hf_xS_2$ was observed in the atmosphere at room temperature by STM. The STM system consists of a STM unit of Angstrom make and a home-built controller. The probe tip was a mechanically cut Pt wire ($\phi = 0.3$ mm). The atomic image of graphite was used for the calibration of the STM system. The surface of the sample was peeled off using an adhesive tape in the air. The STM measurement was performed in variable-current mode with the average tunnelling current about 1 nA and the tip bias -10 mV.

3. Results

All the prepared single crystals of both 1T-TaS_2 and $Ta_{1-x}Hf_xS_2$ were shiny gold-tinted specimens. The atomic ratio of Hf atoms to Ta atoms in the single crystals determined by ICP was much smaller than that of the starting materials sealed in the quartz ampoule for crystal growth. The crystal structure and the lattice constants were measured by the x-ray diffraction (XRD) method. The patterns of the XRD peaks were compared to the simulated ones, and confirmed that the structure of the single crystals obtained was that in which the Hf atoms were substituted for Ta atoms of 1T-TaS_2 crystal. The lattice constants of $Ta_{1-x}Hf_xS_2$ obtained by means of XRD are listed in table 1.

Figures 1(a) and 1(b) show the temperature dependences of the resistivities $\rho(T)$ normalized to each ρ(360 K) for various x in $Ta_{1-x}Hf_xS_2$. Figures 1(c) and 1(d) show the

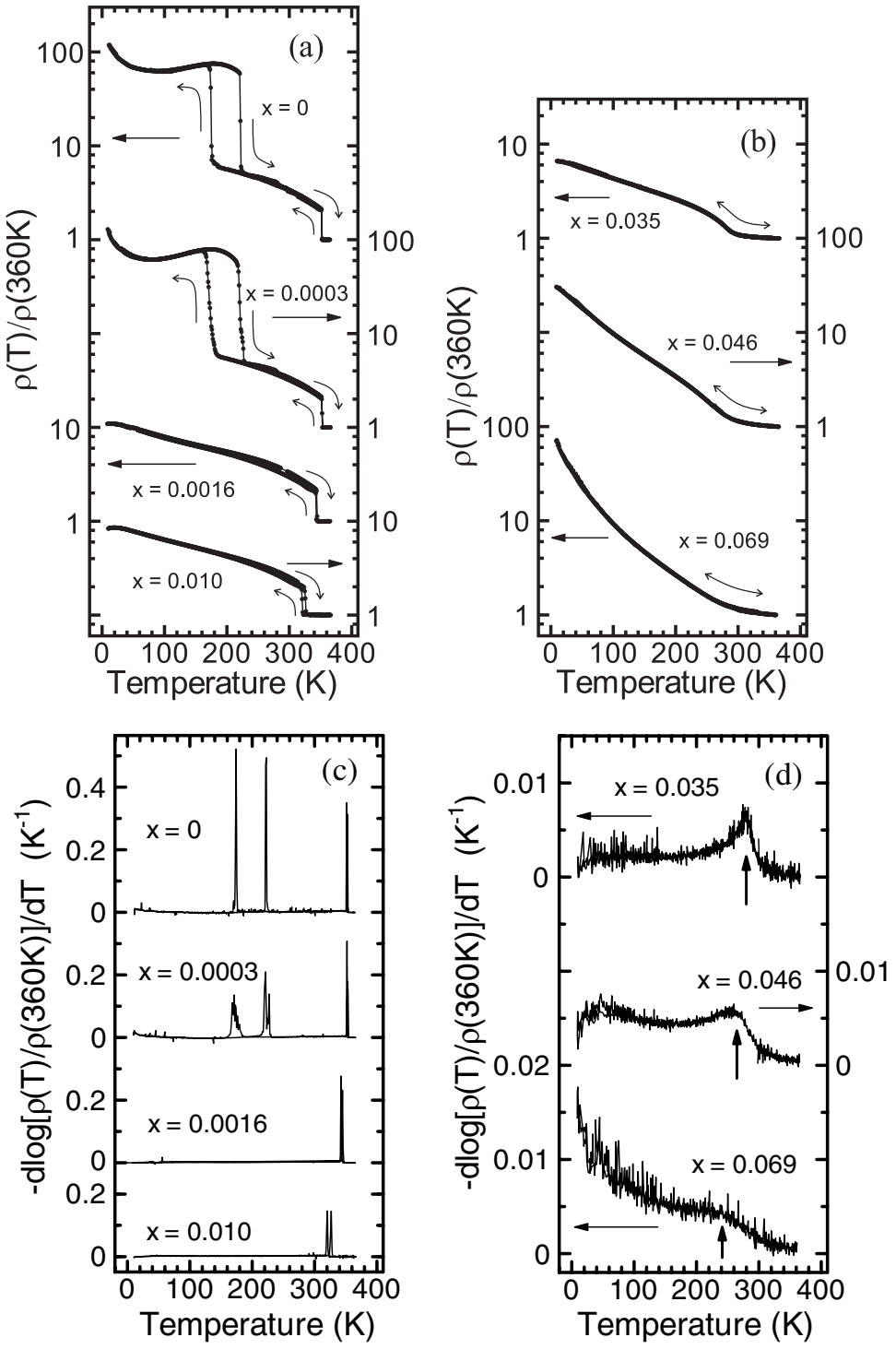

Figure 1. The temperature dependence of the resistivity in $Ta_{1-x}Hf_xS_2$.

Table 1. The lattice constants of $Ta_{1-x}Hf_xS_2$.

x	a (nm)	c (nm)
0	0.3364	0.5898
0.0003	0.3359	0.5898
0.0016	0.3366	0.5898
0.010	0.3371	0.5896
0.035	0.3372	0.5892
0.046	0.3373	0.5892
0.069	0.3382	0.5891

negatives of the derivatives, $-\mathrm{d}\log[\rho(T)/\rho(360\ \mathrm{K})]/\mathrm{d}T$, which correspond to figures 1(a) and 1(b), respectively. The measurements were made about every 1 K. The values of $\rho(360\ \mathrm{K})$ were $\sim 5 \times 10^{-4}\ \Omega$ cm for all samples and they were not changed appreciably by the changes in the Hf concentrations. For $x = 0$, as is known from the previous studies [1, 4–6], two hystereses with jumps of $\rho(T)$ corresponding to the CDW phase transitions were observed in the ρ–T curves. That is, on cooling, 1T-TaS_2 underwent CDW phase transitions from the I phase to the NC phase at 351.9 K and from the NC phase to the C phase at 174.7 K. On heating, it underwent CDW phase transitions from the C phase to the T phase at 221.7 K, from the T phase to the NC phase at 282.8 K (a slight step in the ρ–T curve) and from the NC phase to the I phase at 352.2 K. For $x = 0.0003$, the ρ–T curve was similar to that for $x = 0$. However, the phase transition between the C phase and the NC phase became less sharp than that for $x = 0$. The slopes of the hysteresis curves, $-\mathrm{d}\log[\rho(T)/\rho(360\ \mathrm{K})]/\mathrm{d}T$, in the NC $\rightarrow$ C and the C $\rightarrow$ T CDW phase transitions, were about $0.14\ \mathrm{K}^{-1}$ and $0.21\ \mathrm{K}^{-1}$, respectively. These values are 0.3–0.4 times those for $x = 0$. For $x = 0.0016$, the CDW transition to the C phase vanished in the ρ–T curve. Furthermore, the temperature of the CDW phase transition between the NC and the I phase went down to 342.9 K on cooling and 343.6 K on heating. For $x = 0.010$, it went down further to 320.5 K on cooling and 325.7 K on heating. Thus, the width of the hysteresis curve for the NC–I CDW phase transition became widened to 5.2 K. For $x = 0.035$, 0.046 and 0.069, though the jump and the hysteresis in the ρ–T curve at the NC–I CDW phase transition disappeared, it showed an inflection point, a maximum of $-\mathrm{d}\log[\rho(T)/\rho(360\ \mathrm{K})]/\mathrm{d}T$, at a certain temperature depending on x. This temperature corresponds to the NC–I CDW phase transition for $x \leqslant 0.010$. As x increased, the value of the maximum of $-\mathrm{d}\log[\rho(T)/\rho(360\ \mathrm{K})]/\mathrm{d}T$ became smaller and its temperature decreased. The temperatures were 280.1 K for $x = 0.035$, 264.0 K for $x = 0.046$ and 241.3 K for $x = 0.069$, and these are arrowed in figure 1(d). The dependence of these temperatures on x is shown in figure 2. The error bars of the plots (○) indicate the widths of the hystereses at the NC–I CDW phase transition (for $x \leqslant 0.010$). The triangles plotted indicate the maxima of $-\mathrm{d}\log[\rho(T)/\rho(360\ \mathrm{K})]/\mathrm{d}T$ (for $x \geqslant 0.035$)—that is, the inflection points in the ρ–T curve.

Figure 3 shows the STM images of the CDW state in $Ta_{1-x}Hf_xS_2$. For $x = 0$, the CDW domains and the phase shift of the CDW were observed, which are characteristic of the NC phase [7, 8]. The size of the CDW domain was about 5.9 nm. The rows of the CDW maxima are in phase in three directions oriented at 120° relative to one another, except for the phase shift of the CDW at the domain boundary. This reflects the threefold symmetry of the crystal lattice. Figures 4(a), 4(b) and 4(c) show the CDW domains and the phase shift of the CDW between the adjacent CDW domains by enhancing the contrast of figures 3(a), 3(b) and 3(c) (for $x = 0$, 0.0003 and 0.0016), respectively.

For $x = 0.0003$, the CDW domains and the phase shift of the CDW were observed and the STM images were similar to those for $x = 0$, except for the existence of some CDW

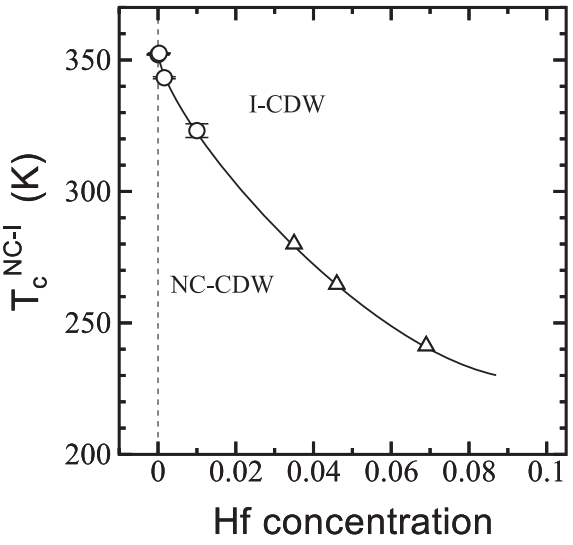

Figure 2. The Hf concentration dependence of the NC–I CDW phase transition temperature T_c^{NC-I}.

defects. The tunnelling current on the defects was much lower than that on the usual CDW minima. Although the position of the CDW defect did not always coincide with the original CDW maximum site, the size of one defect was about the size of one CDW hump. Thus, when the CDW defect occurred at the original CDW maximum site, it looked like just one CDW hump was removed from the site. When the defect lay between the original CDW humps, those CDW humps did not disappear completely. In either case, the CDW defects occurred at the CDW domain boundary. In other words, the CDW domains avoided the CDW defects and were arranged like those for $x = 0$. The size of the CDW domain was about 4.2 nm. The average number of CDW defects was about 0.011 nm^{-2} in the STM images.

For $x = 0.0016$, the CDW domains and the phase shift of the CDW were still observed. The number of CDW defects increased and the size of the CDW defect was larger than that for $x = 0.0003$. The average number of CDW defects was about 0.030 nm^{-2}. The CDW defects still tended to occur at the CDW domain boundary. Hence, the occurrence of the usual CDW domain was suppressed by the CDW defects and the size of the CDW domain became smaller (about 3.2 nm) than those for $x = 0$ and 0.0003 (see figure 4).

For $x = 0.010$, the CDW domains were not observed and the CDW defects were not so distinct as those for $x = 0.0003$ and 0.0016. The phase of the CDW was partially distorted. That is, while there were some areas where the rows of the CDW maxima were in phase in one direction, the rows were broken into short lengths in the other two directions. It is shown in figure 3(d) that the horizontal rows of the CDWs are well aligned, but the rows in the other directions are partially broken and/or bent.

For $x = 0.035$, 0.046 and 0.069, the STM images changed remarkably from those for $x \leqslant 0.010$. An area of a blurred charge-density wave appeared instead of the distinct CDW defect image such as is seen in the STM images for $x = 0.0003$ and 0.0016. The phase of the CDW was disturbed and the CDW state lost the original threefold symmetry. The coherence length of the CDW became remarkably shorter than that for $x \leqslant 0.010$. Though there remained some CDW humps, the other CDWs were connected to form a line structure in the STM images (a line structure of the CDWs).

For $x = 0.035$ (figure 3(e)), there remained more CDW humps in the STM image than for $x = 0.046$ and 0.069. The directions of the line structures of the CDWs could be

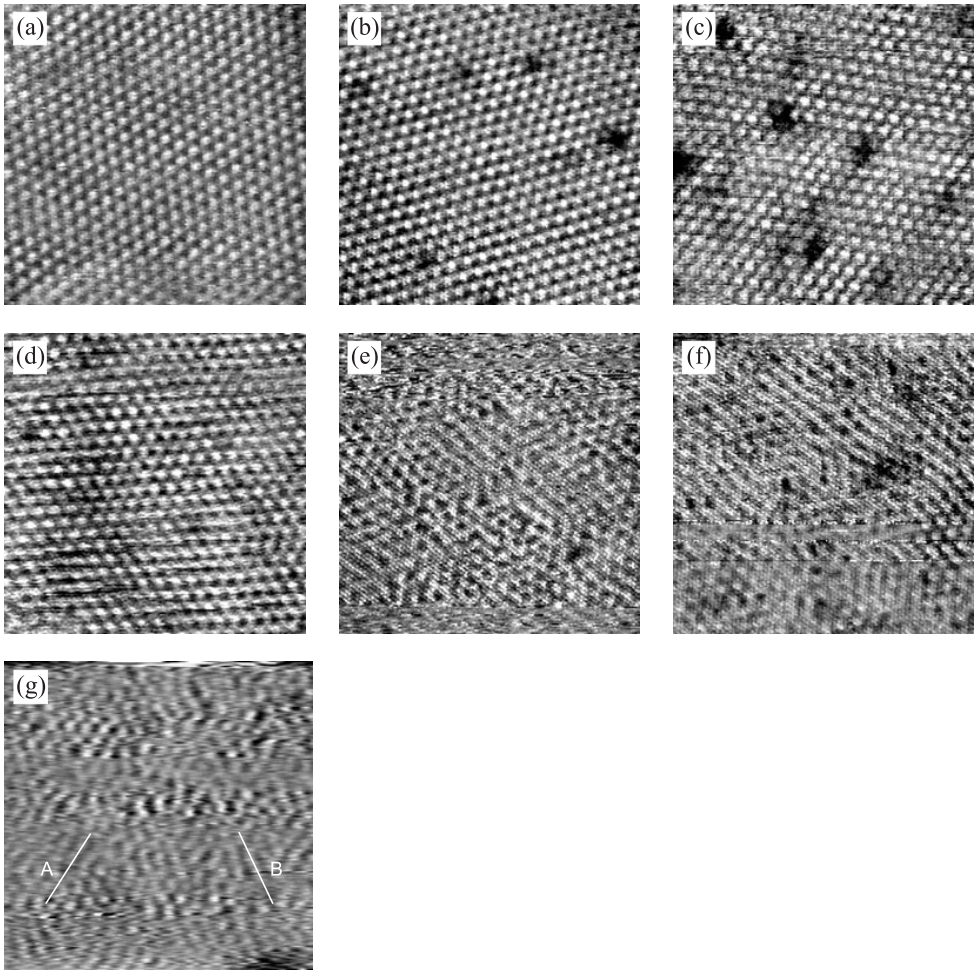

Figure 3. The STM images for $Ta_{1-x}Hf_xS_2$ at room temperature in 23×23 nm^2. (a) $x = 0$, (b) $x = 0.0003$, (c) $x = 0.0016$, (d) $x = 0.010$, (e) $x = 0.035$, (f) $x = 0.046$ and (g) $x = 0.069$.

roughly grouped into three directions. These directions were nearly parallel to the alignment of the atoms.

For $x = 0.046$ (figure 3(f)), a major line structure of the CDWs appeared in one direction (from the top to the right in figure 3(f)) and those in the other two directions were weak.

For $x = 0.069$ (figure 3(g)), the directions of the line structures of the CDWs were roughly grouped into two directions denoted with 'A' and 'B' in figure 3(g). These features are clearly shown by 2D Fourier-transformed images mentioned below.

Figure 5 shows STM images in small areas: (a) 6×6 nm^2 for $x = 0.0003$, (b) 6×6 nm^2 for $x = 0.035$, (c) 12×12 nm^2 for $x = 0.046$ and (d) 12×12 nm^2 for $x = 0.069$. The small light spots represent the outermost S atoms and the white clusters of them represent the CDW humps. These STM images clearly show the relative arrangements of the S atoms and the CDWs. For $x = 0.0003$ (figure 5(a)), the translation vectors of the CDW superlattice ($\boldsymbol{a}^{\mathrm{CDW}}$ and $\boldsymbol{b}^{\mathrm{CDW}}$) are expressed as $\boldsymbol{a}^{\mathrm{CDW}} = 3\boldsymbol{a} - \boldsymbol{b}$ and $\boldsymbol{b}^{\mathrm{CDW}} = \boldsymbol{a} + 4\boldsymbol{b}$ ($\boldsymbol{a}$, $\boldsymbol{b}$: primitive axes of the atomic lattice) and thus the CDW is commensurate with the atomic lattice. Therefore, the angle

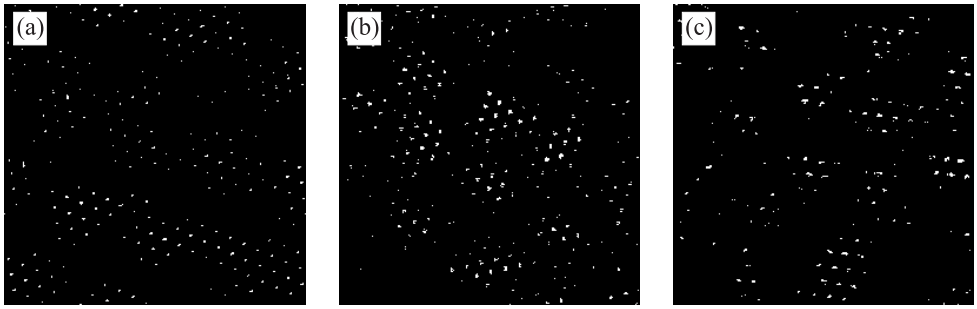

Figure 4. The STM images of figures 3(a), 3(b) and 3(c) with enhanced contrast.

between the atomic lattice and the CDW superlattice is 13.9°. This indicates that the whole field of the image is within a CDW domain. On the other hand, for $x = 0.035$ (figure 5(b)), the directions of the line structures of the CDWs fluctuate, but they are nearly parallel to the atomic lattice, which is a feature of the I-CDW phase. Figure 5(c), for $x = 0.046$, shows that the line structure of the CDWs is composed of about 4–5 CDWs and that the directions of the main lines are also nearly parallel to the atomic lattice. Figure 5(d), for $x = 0.069$, shows that the line structures of the CDWs are continuously curved, and thus the angle between the

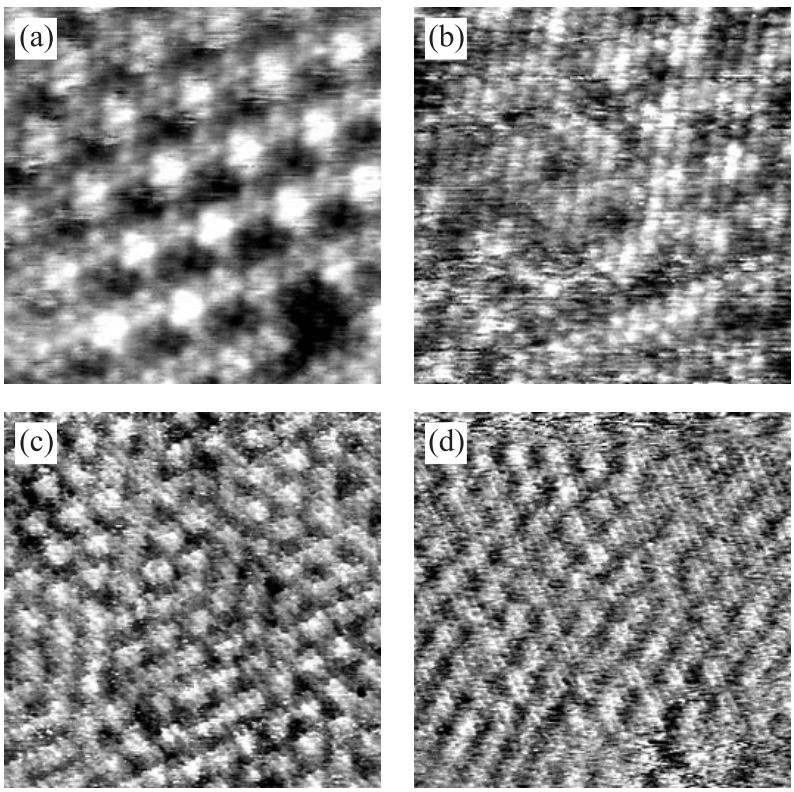

Figure 5. The STM images of $Ta_{1-x}Hf_xS_2$. (a) $x = 0.0003$ in 6×6 nm^2. (b) $x = 0.035$ in 6×6 nm^2. (c) $x = 0.046$ in 12×12 nm^2. (d) $x = 0.069$ in 12×12 nm^2.

atomic lattice and the line structures of the CDWs becomes variable to some extent.

Figures 6(a)–6(g) show the 2D Fourier-transformed (2DFT) images of the STM images in figures 3(a)–3(g), respectively. In figure 6(a), the spots for the atomic lattice ($\boldsymbol{q}_i^{\mathrm{lat}}$; $i = 1, 2, 3$) and those for the CDW superlattice ($\boldsymbol{q}_i^{\mathrm{CDW}}$) are denoted with 'L' and 'C', respectively.

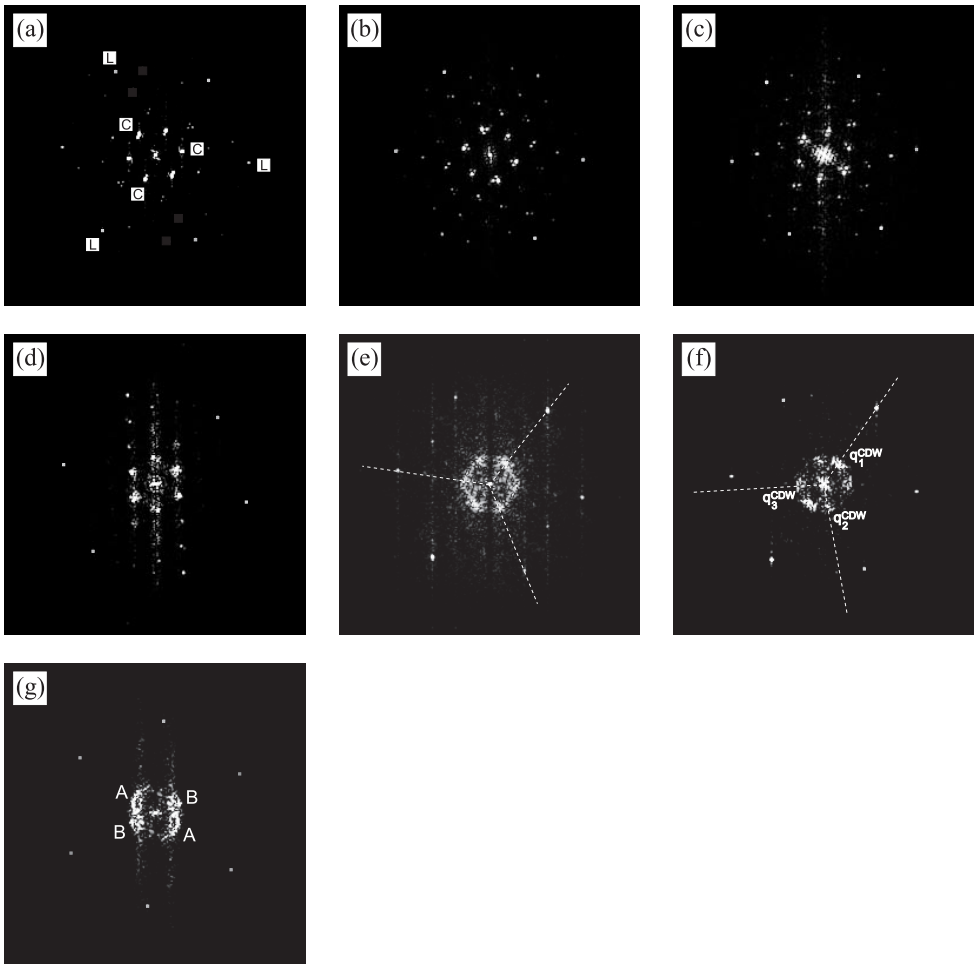

Figure 6. The 2D Fourier-transformed images of the STM images in figure 3. (a) $x = 0$, (b) $x = 0.0003$, (c) $x = 0.0016$, (d) $x = 0.010$, (e) $x = 0.035$, (f) $x = 0.046$ and (g) $x = 0.069$.

For $x = 0$, 0.0003 and 0.0016, the resulting 2DFT images showed similar patterns: the six spots for the atomic lattice, the six main spots for the CDW superlattice and the satellite spots for the CDW domain superlattice around the CDW spots. The absolute values, $|\boldsymbol{q}_i^{\mathrm{CDW}}|$, of the $\boldsymbol{q}_i^{\mathrm{CDW}}$ were $\sim 0.28|\boldsymbol{q}_i^{\mathrm{lat}}|$ and the angles between the $\boldsymbol{q}_i^{\mathrm{CDW}}$ and the $\boldsymbol{q}_i^{\mathrm{lat}}$ were $\sim 12^\circ$. Because the 2DFT image averages the angle between the CDW superlattice and the atomic lattice including the phase shift of the CDW, the value 12° is different from the value 13.9° mentioned above. The values 0.28° and 12° have uncertainties of $\sim 0.01^\circ$ and $\sim 1^\circ$, respectively, because the values were calculated by using the digital coordinates of the computer, but these values agreed with the results from the electron and the x-ray diffraction for 1T-TaS_2 [1, 18].

For $x = 0.010$, the 2DFT pattern was similar to those for $x \leqslant 0.0016$ except for the absence

of the satellite spots for the CDW domain. The satellite spots for the CDW superlattice formed a linear pattern in the vertical direction. This corresponds to the STM image (figure 3(d)), in which the CDW row is most distinct in the horizontal direction as mentioned above.

For $x = 0.035$, 0.046 and 0.069, the 2DFT patterns became remarkably different from those for $x \leqslant 0.010$. The three corresponding dashed lines are drawn in figures 6(e) and 6(f), respectively. These lines denote the directions of $\boldsymbol{q}_i^{\mathrm{CDW}}$. The spots for the CDW became blurred along the circumference with a radius nearly equal to $0.28|\boldsymbol{q}_i^{\mathrm{lat}}|$, while the spots for the atomic lattice remained spots with a hexagonal arrangement. This means that the wavelengths of the CDW for $x \geqslant 0.035$ are near to that for $x = 0$ but the directions of the CDW wave vectors are varied.

For $x = 0.035$, the $\boldsymbol{q}_i^{\mathrm{CDW}}$ changed to $\sim 0.28\boldsymbol{q}_i^{\mathrm{lat}}$. That is, the directions of the $\boldsymbol{q}_i^{\mathrm{CDW}}$ became nearly parallel to those of the $\boldsymbol{q}_i^{\mathrm{lat}}$, with the absolute values kept unchanged within the accuracy mentioned above.

For $x = 0.046$, the $|\boldsymbol{q}_i^{\mathrm{CDW}}|$ did not change but the directions of the $\boldsymbol{q}_i^{\mathrm{CDW}}$ relative to the $\boldsymbol{q}_i^{\mathrm{lat}}$ changed from those for $x = 0.035$. Though $\boldsymbol{q}_1^{\mathrm{CDW}}$, for which the intensity was strongest among those for the three $\boldsymbol{q}_i^{\mathrm{CDW}}$, was nearly parallel to $\boldsymbol{q}_1^{\mathrm{lat}}$, the angles between $\boldsymbol{q}_i^{\mathrm{CDW}}$ and $\boldsymbol{q}_j^{\mathrm{CDW}}$ ($i, j = 1, 2, 3$) were not 120° but 135° between $\boldsymbol{q}_1^{\mathrm{CDW}}$ and $\boldsymbol{q}_2^{\mathrm{CDW}}$, 97° between $\boldsymbol{q}_2^{\mathrm{CDW}}$ and $\boldsymbol{q}_3^{\mathrm{CDW}}$, 128° between $\boldsymbol{q}_3^{\mathrm{CDW}}$ and $\boldsymbol{q}_1^{\mathrm{CDW}}$.

Furthermore, for $x = 0.069$, though the spots for the atomic lattice remained hexagonal, the pattern for the CDW had the two main areas denoted with 'A' and 'B' in figure 6(g) instead of the six spots observed for the smaller-x samples.

4. Discussion

It is important to compare the present results for Hf substitution to the previous results for Ti substitution [11]. The Ti–S bond length (0.242 nm in 1T-TiS_2 [15]) is near to the Ta–S bond length (0.244 nm in 1T-TaS_2 [15]); thus, the lattice distortion caused by the substitution of Ti for Ta is very small. Furthermore, the energy levels of the d orbitals of Ti and Ta are close to each other [14]. Thus, Ti atoms can be substituted for Ta atoms to a high concentration [4, 10]. These facts mean that the wave functions of the 3d orbitals of Ti are well hybridized with the 5d orbitals of Ta and are delocalized, and that the effect of the substitution is a shift of the Fermi level depending on the number of d electrons. Thus, the Ti substitution reduces the number of electrons by one per Ti atom and it changes the nesting conditions for the occurrence of the CDW owing to the shrinkage of the Fermi surface. This effect makes the wavelength of the CDW longer [1, 11]. Therefore, the Ti atom acts as a weak pinning centre for the CDW in 1T-TaS_2.

On the other hand, the Hf–S bond length (0.256 nm in 1T-HfS_2 [15]) is much larger than the Ta–S bond length in 1T-TaS_2. Moreover, the energy levels of the 5d orbitals of Hf are much higher than those for Ta [14], though the number of d electrons of Hf is less than that of Ta by one, similarly to the case for Ti. These two factors lead to a CDW defect state having a local lattice distortion and a local electron deficiency around the Hf site within a certain radius. Then, the CDW defect caused by the Hf atom does not affect the CDW state outside the CDW defect. Hence, the Hf atoms do not change the Fermi level outside the CDW defect and, thus, the $|\boldsymbol{q}_i^{\mathrm{CDW}}|$ are not changed by the Hf doping, in contrast to the case for the Ti doping. The free energy in the area outside the CDW defects is lower in the CDW state than that in the normal state. The CDW state profits the free energy by causing distortion of the lattice with $\boldsymbol{q}_i^{\mathrm{CDW}}$ accompanied by the formation of the energy gap at the Fermi level. Therefore, if a Hf atom lies in the CDW state region, the local lattice distortion around the Hf atom disturbs

the periodic lattice distortion in the CDW state and the CDW state loses free energy. Thus, it is more advantageous for the CDW state to accommodate the Hf-related distortion at the domain boundary, where the amplitude of the periodic lattice distortion caused by the CDW is small. Then, avoiding the CDW defects outside the CDW domain is more advantageous than including the CDW defects within the CDW domain. Therefore, the CDW domain boundary tends to lie on the CDW defects and thus the Hf atom acts as a strong pinning centre for the CDW domain boundary.

We compare the results from the STM images with the ρ–T results. For the pure 1T-TaS_2, it is known that the size of the CDW domain increases on cooling, and at the temperature of the NC $\rightarrow$ C CDW phase transition, the CDW domains combine together and the whole area of the crystal plane becomes part of the C phase [3]. Within the C-phase area, the conduction electrons are localized into the Star-of-David cluster of the 13 Ta atoms (the CDW hump) and the electrical resistivity becomes very high. In the NC-CDW phase, the resistivity can be as low as $1/10$ of that in the C phase (figure 1), because the electrons are not localized within the CDW domain boundary.

For $x = 0.0003$, the CDW domains of the NC phase can avoid the CDW defects caused by Hf atoms without reducing the size of the CDW domain, because the concentration of the CDW defects is low enough. In this case, on cooling, the domains can unite with one another and form a C phase over the whole sample plane, leaving the point CDW defects in the C phase.

For $x = 0.0016$, the separation of the CDW defects is smaller. Then, the size of the CDW domain is reduced in order to avoid the CDW defects. In such a case, the CDW domains cannot unite with one another to form the C phase, and the ρ–T curve does not show the NC $\rightarrow$ C CDW phase transition.

For $x = 0.0003$ and 0.0016, we can count the number of CDW defects in the STM images. It was always 2–4 times more than that estimated from the value of x. This discrepancy is not understood, but we assume that the Hf atoms in a few surface layers affect the STM image.

For $x \geqslant 0.035$, the CDW domain structure itself cannot be formed because of the high defect concentration. In this case, the ρ–T curve does not show a distinct NC–I CDW phase transition but shows an inflection point. The temperature of the inflection point lies below room temperature for these x-values. This fact is consistent with the 2DFT result that for these x-values, the $\boldsymbol{q}_i^{\mathrm{CDW}}$ are parallel to the $\boldsymbol{q}_i^{\mathrm{lat}}$, which is a characteristic of the I-CDW.

5. Conclusions

The effect of doping with Hf atoms on the NC-CDW structures of 1T-TaS_2 was investigated using STM at room temperature. Hf was substituted for Ta in 1T-TaS_2 up to 6.9%. It was found that the Hf atom introduces a point defect into the CDW superlattice at the CDW domain boundary for lower contents. Thus, the Hf atom acts as a strong pinning centre for the CDW domain boundary. For Hf contents higher than 1%, the CDW superlattice melted and a distorted structure was observed instead of the usual CDW superlattice. The change of the CDW structure observed by STM was also analysed using their 2DFT images. The change of the CDW structure was compared with the change of the ρ–T characteristics.

Acknowledgment

This work was partially supported by a Waseda University Grant for a Special Research Project (98A-141).

References

[1] Wilson J A, DiSalvo F J and Mahajan S 1975 *Adv. Phys.* **24** 117
[2] Thomson R E, Walter U, Ganz E, Clarke J, Zettl A, Rauch P and DiSalvo F J 1988 *Phys. Rev.* B **38** 10 734
[3] Thomson R E, Burk B, Zettl A and Clarke J 1994 *Phys. Rev.* B **49** 16 899
[4] DiSalvo F J, Wilson J A, Bagley B G and Waszczak J V 1975 *Phys. Rev.* B **12** 2220
[5] DiSalvo F J and Graebner J E 1977 *Solid State Commun.* **23** 825
[6] Tani T, Okajima K, Itoh T and Tanaka S 1981 *Physica* B **105** 127
[7] Wu X L and Lieber C M 1989 *Science* **243** 1703
[8] Coleman R V, McNairy W W and Slough C G 1992 *Phys. Rev.* B **45** 1428
[9] DiSalvo F J, Wilson J A and Waszczak J V 1976 *Phys. Rev. Lett.* **36** 885
[10] Thompson A H, Pisharody K R and Koehler R F 1972 *Phys. Rev. Lett.* **29** 163
[11] Wu X L, Zhou P and Lieber C M 1988 *Phys. Rev. Lett.* **61** 2604
[12] Chen H, Wu X L and Lieber C M 1990 *J. Am. Chem. Soc.* **112** 3326
[13] Dai H and Lieber C M 1993 *J. Phys. Chem.* **97** 2362
[14] Grasso V 1986 *Electronic Structure and Electronic Transitions in Layered Materials* (Dordrecht: Reidel) p 6
[15] Gamble F R 1974 *J. Solid State Chem.* **9** 358
[16] Fujimoto H and Ozaki H 1984 *Solid State Commun.* **49** 1117
[17] Bando H, Miyahara Y, Enomoto H and Ozaki H 1997 *Surf. Sci.* **381** L609
[18] Scruby C B, Williams P M and Parry G S 1975 *Phil. Mag.* **31** 255